J Mater Sci: Mater Electron (2021) 32:3863–3877

Study of the effect of ion irradiation on increasing the photocatalytic activity of WO_3 microparticles

Artem L. Kozlovskiy[1,2,*], Alua Alina[1], and Maxim V. Zdorovets[1,2,3]

[1] *Engineering Profile Laboratory, L.N. Gumilyov Eurasian National University, Nur-Sultan 010008, Kazakhstan*
[2] *Laboratory of Solid State Physics, The Institute of Nuclear Physics, Almaty 050032, Kazakhstan*
[3] *Department of Intelligent Information Technologies, Ural Federal University, Yekaterinburg, Russia 620075*

Received: 4 November 2020
Accepted: 15 December 2020
Published online: 12 January 2021

ABSTRACT

The work is devoted to the study of the possibility of using low-energy irradiation with helium ions to increase the photocatalytic activity of tungsten oxide (WO_3) microparticles, if used as catalysts for the decomposition of Rhodamine B. The prospect of this study is to find new ways to solve the problem of increasing the catalytic activity of micro- and nano-particles. During the study, the dependences of changes in the structural and morphological properties of the studied microparticles exposed to irradiation were established, and the effect of irradiation on the increase in the efficiency of decomposition of the organic dye Rhodamine B in aqueous media under UV irradiation was studied. It was found that the use of irradiation with helium ions leads to an increase not only in the rate of photocatalytic reactions, but also in the degree of mineralization, as well as in the efficiency of removing COD from aqueous solutions. Cyclic tests have shown the resistance of the modified microparticles to degradation, as well as the retention of the decomposition efficiency, with a decrease in the degree of mineralization after ten test cycles by 30%. At the same time, unlike the initial microparticles, ionic modification leads to an increase in the resistance of the structure to temporary degradation during cyclic tests.

1 Introduction

Today, one of the most pressing environmental problems is the wastewater treatment of the textile and light industries, in the production of which a huge amount of organic dyes is used to dye fabrics, paper, etc. The use of new dyes, such as indigo carmine, Rhodamine B, etc., which have good indicators of light fastness, brightness, opened up new opportunities for the production of printing, textiles, pigment production, etc [1–5]. However, in spite of their active use, the processes of utilization of these dyes are rather laborious and energy-consuming, and the accumulation of dyes in high concentrations can lead to pollution and mutagenic effects on the environment [6, 7]. However, in most cases, the use of standard physical or chemical methods for the separation or removal of organic dyes is not applicable or

Address correspondence to E-mail: kozlovskiy.a@inp.kz

https://doi.org/10.1007/s10854-020-05130-8

ineffective. This is primarily due to the fact that most dyes have high resistance to chemical attack, radiation, degradation, insolubility in water, etc [8–10].

In the recent decades, to solve this problem and increase the efficiency of the utilization of organic dyes and their wastes, methods for photocatalytic decomposition under the influence of UV radiation using metal nano- and microstructures, as well as their oxide compounds as photocatalysts, have been proposed [11–15]. At the same time, structures based on ZnO [16–19], CuO [20, 21], GaO [22, 23] Cd, Se, and their various compounds with ferrite structures [24–30], as well as various magnetic nanoparticles based on iron oxides or niodymium [31–34] have found wide application in this field. Interest in these types of nano- and micro-structures is due to their unique structural, optical, magnetic or conductive properties, which make them promising materials not only in photocatalysis, but also in other fields of science and technology [35–38]. So, for example, for the decomposition of Rhodamine B in aqueous media Ahmad et.al. [39], it was proposed to use composite structures based on zinc oxide and carbon nanotubes (ZnO/CNTs), which during the study showed high efficiency not only in dye degradation, but also in mineralization and in lowering Chemical oxygen demand. And in the work of Mahadik et al. [40] showed the promise of the use of nanostructured thin films based on titanium oxide (TiO_2) and iron oxide (Fe_2O_3) for the photocatalytic degradation of Rhodamine B. Most of the studies on the photocatalytic reactions of dye degradation pay great attention to the size of the catalysts. So, for example, in a series of works by Martinez-de la Cruz et al. [41–43] showed that a decrease in the size of WO_3 nanoparticles leads not only to an increase in the efficiency of photocatalytic decomposition, but also to a significant increase in the reaction rate. It is worth noting that to increase the efficiency of photocatalysts, various modifications of structural and morphological properties are also used, such as doping with rare earth elements [44–46], adding carbon nanotubes or fullerenes to the composition [36, 47, 48], thermal or ionic effects [49, 50]. In this case, the main goal of any modification methods is to change the surface morphology of the photocatalyst, which plays an important role in heterogeneous catalysis. An increase in the active surface area due to grain size changes or dislocation density can create additional activation centers capable of participating in photocatalytic decomposition. One of the effective ways to change the surface morphology is to irradiate with low-energy ions with large fluencies. In this case, the low energy of the incident particles and the predominance of nuclear energy losses during inelastic collisions lead to the formation of a large number of atomic displacements in a small surface layer with a thickness of no more than 250–300 nm [51, 52]. In this case, large irradiation fluences (10^{14}–10^{15} ion/cm^2) lead to the formation of the effect of overlapping defective regions, which enhances the efficiency of changing the morphology of the surface layer, while the inner bulk of the photocatalyst itself remains unchanged.

Based on the foregoing, the aim of this work is to study the possibility of using low-energy helium ions to modify the near-surface layer of WO_3-based microparticles and increase the photocatalytic activity and degree of mineralization in the decomposition of the organic dye Rhodamine B in water under the influence of UV radiation. The choice of ionizing radiation in the form of helium and fluence ions 1×10^{15} ion/cm^2 is due to the possibility of modeling the processes of defect formation and their overlap in the structure of the surface layer in order to increase the density of dislocation defects and change the specific surface area.

The novelty of this study consists in expanding the possibilities of using ionizing radiation as one of the methods for modifying nano- and micro-particles, as well as the possibility of increasing the efficiency of photocatalytic properties of oxide micro- and nanoparticles. At the same time, the choice as the basis for photocatalysts of commercial WO microparticles is due to a large number of promising studies aimed not only at studying the structural, optical and electronic properties of WO micro- and nano-particles, but also at finding methods for modifying their properties using various methods, including irradiation with ionizing radiation. At the same time, high resistance to degradation, oxidation processes, as well as temperature differences and heating up to 700–900 °C, the width of the forbidden zone 2.4–3 eV, the electronic structure makes WO_3-based structures one of the promising materials not only for photocatalysis, but also for gas-sensitive sensors, semiconductor devices for determining harmful and explosive gases and substances, etc. At the same time, in most practical applications to nano- and micro-structures, requirements are put forward for increased resistance to degradation, as well as duration of operation and

preservation of stability of performance. In turn, modification with ionizing radiation allows increasing resistance to degradation, as well as making significant changes in the optical and electronic properties of structures, thereby changing photocatalytic activity. The relevance of the study lies in the search for new opportunities to increase the photocatalytic activity of oxide micro- and nanoparticles, which will further increase the productivity not only of the degree of purification, but also of the number of cycles of use.

2 Experimental technique

The initial samples were WO_3 microparticles manufactured by Sigma Aldrich (St. Louis, Missouri, USA), with a monoclinic type of crystal lattice, with a spatial syngony P21/n(14). The choice of these microparticles is due to their wide use as a basis for photocatalysts, high resistance to degradation and decomposition, which allows them to be used a sufficiently large number of times in photocatalysis.

Irradiation with low-energy helium ions (He^{2+}) with an energy of 40 keV was carried out at the DC-60 heavy ion accelerator (Nur-Sultan, Kazakhstan) with an irradiation dose of 1×10^{15} ion/cm^2 [53, 54]. Previously, we carried out a detailed study of the processes of radiation damage during irradiation with helium ions, as well as the subsequent processes of swelling and changes in the surface morphology of microparticles. In [54], structural and morphological changes during the accumulation of radiation damage are considered in detail, and the mechanisms of their origin are proposed. At the same time, one of the important results obtained by us was the fact that under irradiation with doses of 10^{15} ion/cm^2, a change in surface morphology is observed, leading to partial fragmentation of grains and an increase in the active surface area. These structural changes can be used to increase the photocatalytic activity, as well as to change the rate of the dye decomposition reaction and the degree of mineralization.

The study of changes in the morphological features of microparticles before and after irradiation, as well as degradation after photocatalytic reactions, was carried out using scanning electron microscopy [Hitachi TM4000 scanning electron microscope (Hitachi Ltd., Chiyoda, Tokyo, Japan)] and transmission electron microscopy (TEM microscope JEM 2100 LaB_6 or ARM200F, JEOL, Ltd., Tokyo, Japan).

The kinetics of changes in structural characteristics was evaluated by X-ray diffractometry performed on a D8 Advance Eco powder diffractometer (Bruker, Karlsruhe, Germany). The diffraction patterns were recorded in the Bragg–Brentano geometry at $2\theta = 20°–50°$, in increments of $2\theta = 0.01°$, and the spectra were taken at 3 s. The analysis of the obtained diffraction patterns was carried out using the DiffracEva 4.2 software.

Optical properties and determination of optical characteristics were carried out by analyzing the UV–Vis spectra of the synthesized ceramics, recorded on a Jena Specord-250 BU analytical spectrophotometer. Shooting mode 350–1000 nm with a resolution of 1 nm.

The photocatalytic properties of WO_3 microparticles were evaluated by the decomposition of the organic dye Rhodamine B in water under the influence of UV radiation. A box made of borosilicate glass immersed in a water bath to maintain room temperature during processing with a xenon lamp (2100 lm) was used as a photochemical reactor. The test interval was 300 min in increments of 30 min. The concentration of WO_3 microparticles was 10 mg/L. Initial dye concentrations were 30 mg/L for Rhodamine B. To prevent the accumulation of sediment at the bottom of the box as a result of catalyst agglomeration, vigorous stirring of the solution was used.

Determination of photocatalytic properties was carried out using UV–Vis spectroscopy methods, by taking UV–Vis spectra in the range 400–700 nm, with a step of 1 nm. This region is characterized by the presence of an absorption maximum at 554–556 nm, characteristic of Rhodamine B. The change in the intensity of the maximum made it possible to assess the degree of degradation of Rhodamine B by comparing the change in the intensity value over time with the initial value.

3 Results and discussion

Figures 1, 2 and 3 show the results of changes in the morphology of WO_3 microparticles as a result of irradiation, obtained using SEM and TEM. The detailed description of structural and morphological

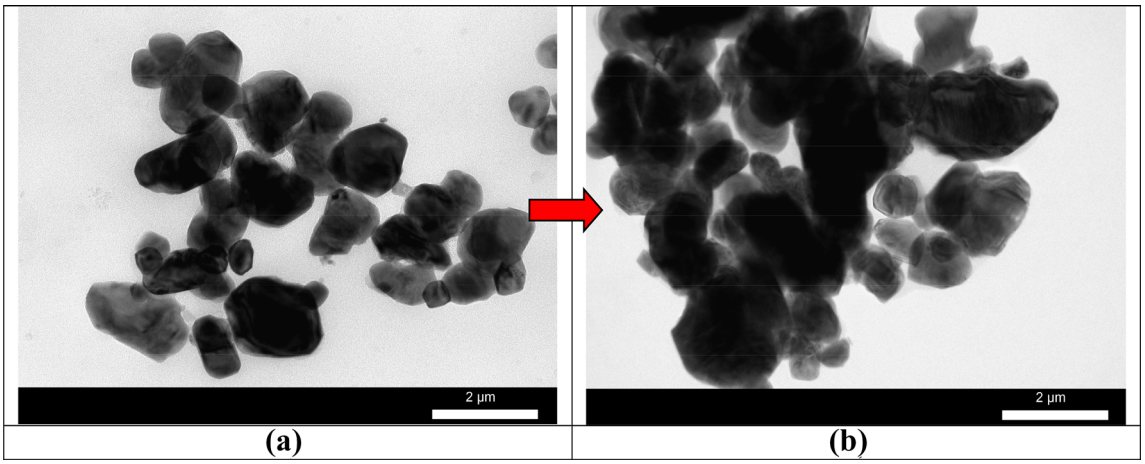

Fig. 1 TEM images: **a** initial sample; **b** irradiated 1×10^{15} ion/cm^2

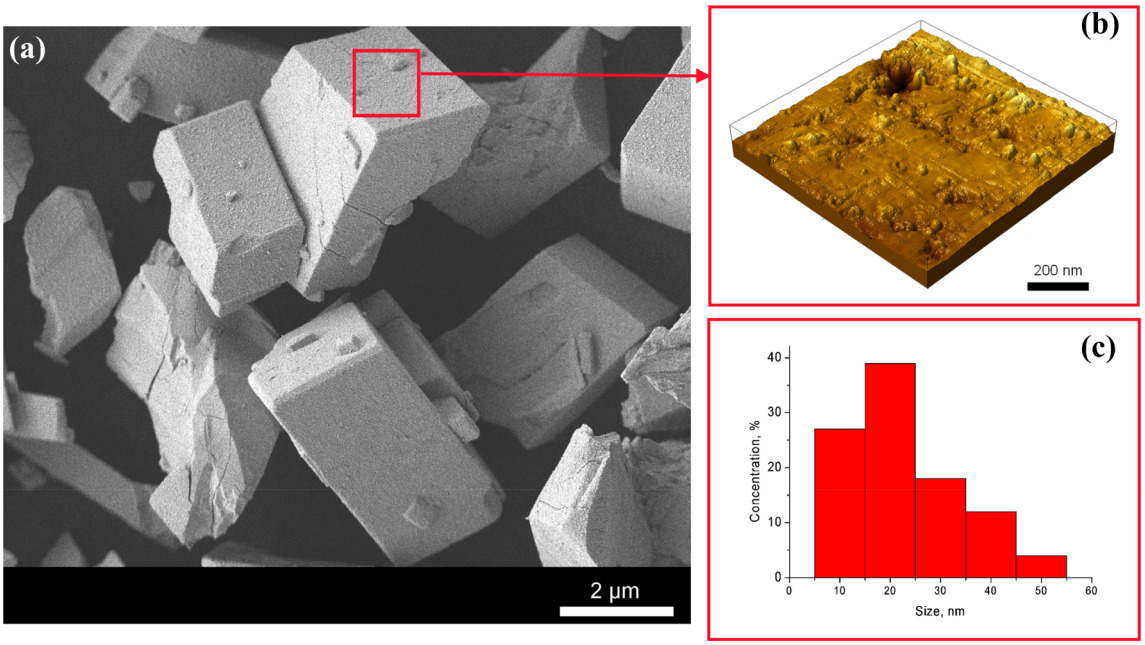

Fig. 2 **a** SEM image of WO_3 microparticles in the initial state; **b** 3D image of the morphology of microparticles; **c** dynamics of changes in the size of inclusions on the surface of microparticles

changes in microparticles under irradiation is presented in [54].

Figures 2 and 3 show the results of the study of morphological features of the analysed microparticles before and after ionic modification. In the initial state, the analysed microparticles are cubic or rectangular particles, the average sizes of which vary from 3 to 5 microns. In a detailed analysis of the surface of microparticles, it was found that they consist of their nanoscale grains whose size does not exceed 20–25 nm. Moreover, according to TEM data, the structure of the initial microparticles is isotropic, in contrast to the irradiated microparticles, for which the surface layer has insignificant differences compared with the initial structures.

As can be seen from the data in Fig. 3, the surface layer of irradiated microparticles is a porous structure with a significant degree of roughness (more than 15–20 nm, and waviness of 19–26 nm), and an increase in the dispersion of grain sizes of the surface is observed, with an average value shifting in the diagram of the Fig. 3c to the region of large values. A change in the morphology of the surface layer indicates that during irradiation the released energy from

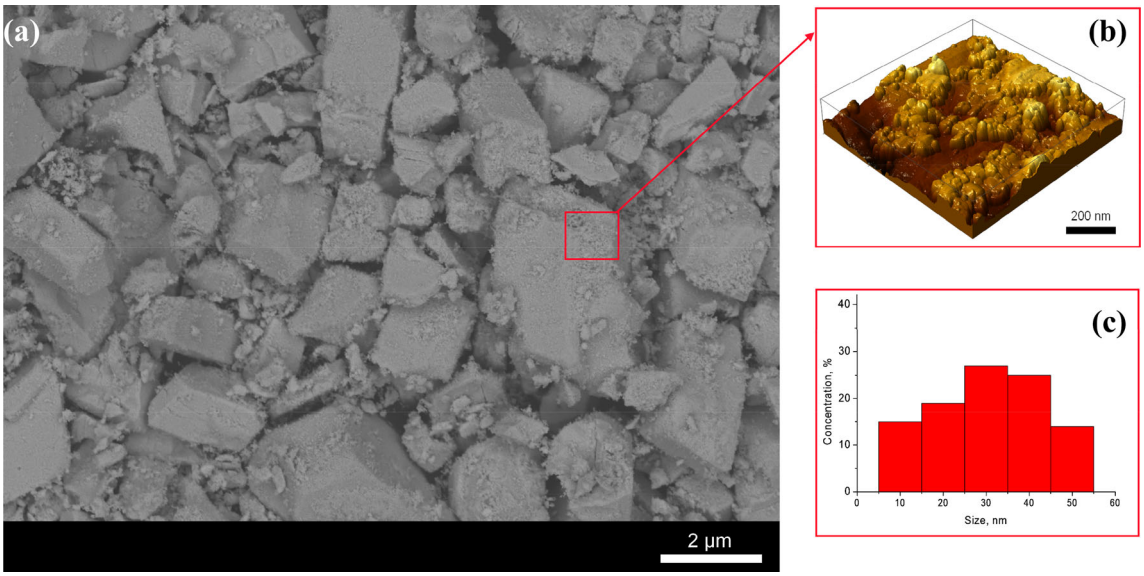

Fig. 3 **a** SEM image of WO_3 microparticles after irradiation with a dose of 1×10^{15} ion/cm^2; **b** 3D image of the morphology of microparticles; **c** dynamics of changes in the size of inclusions on the surface of microparticles

the incident particles led to a partial degradation of the surface layer and its fragmentation, while it can be seen that the main inner part of the microparticles remains unchanged, which indicates that the irradiation changes only the surface layer. At the same time, the change in grain sizes, as well as the formation of a porous layer as a result of irradiation, can have a significant effect on the change in structural and optical characteristics, which play an important role in catalytic properties.

Figure 4 shows the dynamics of changes in the structural parameters of the studied WO_3 microparticles before and after irradiation, obtained by analyzing X-ray diffraction patterns. The lattice parameters were determined by approximating the diffraction lines, followed by subtracting Cu-kλ_2 and comparing the positions of the diffraction lines with the reference values for the WO_3 phase PDF-01-073-6498. The parameters were refined using the main diffraction maxima characteristic of each crystal lattice parameter. The density of the microparticles was determined by X-ray method using the formula (1):

$$p = \frac{1.6602 \sum AZ}{V_0}, \tag{1}$$

where V_0 is the volume of the unit cell, Z is the number of atoms in the crystal cell, A is the atomic weight of the atoms. The crystallite size was determined using the Williamson–Hall technique by refining the shape of the diffraction lines and their distortion. In the case of irradiated samples, where distortions and deformations of the structure contribute mainly to the shape change of the diffraction lines, the use of this technique gives a more accurate result than the standard crystallite sizing technique using the Scherrer equation. The specific surface area

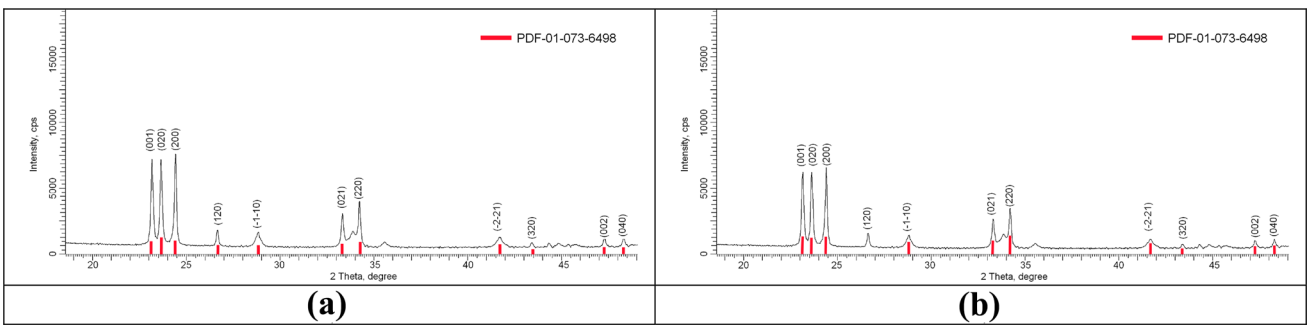

Fig. 4 X-ray diffraction patterns of WO_3 microparticles: **a** initial sample; **b** irradiated 1×10^{15} ion/cm^2

was determined by the Brunauer–Emmett–Teller adsorption method. Integral porosity was determined as the difference between the densities of the test sample and the reference density for this sample according to the PDF2 database. Table 1 shows the changes in the crystallographic parameters of the microparticles under study before and after irradiation.

As can be seen from the data presented, irradiation leads to a distortion of the crystal lattice parameters due to the occurrence of defects during irradiation and their subsequent migration, which leads to crushing of crystallites and an increase in porosity. Thus, the irradiation effect is associated not only with a change in the surface morphology and the formation of porous inclusions and an increase in roughness, but also with a change in the crystallographic characteristics leading to distortion of the structure and the appearance of defective regions, as evidenced by a change in the shape of the main diffraction lines and a decrease in intensity. The deformation of the crystalline structure, as well as a decrease in the size of crystallites, indicates a change in the dislocation density of defects, which increases due to grain fragmentation, as well as their reorientation and the appearance of new grain boundaries.

Using the method of approximating diffraction lines by a set of pseudo-Voigt functions, the degree of perfection of the crystal structure of the studied microparticles before and after ionic modification was determined, the changes in which are presented in Table 1. For the initial microparticles, the degree of crystallinity was 93.3%, which indicates a high degree of structural ordering and low concentration of defects. In the case of irradiated microparticles, a slight decrease in the value of the degree of crystallinity to 92.1% was observed, which indicates a change in the concentration of defects in the structure, which is confirmed by the data of transmission and scanning electron microscopy.

Figure 5 shows the UV–Vis measurement of the transmission spectra of the examined microparticles before and after irradiation, as well as Tauc's plot, on the basis of which the value of the band gap (E_g) was calculated. As can be seen from the data presented, the irradiation results in a slight decrease in the transmittance in the region of 500–1000 nm, as well as a shift in the edge of the fundamental absorption, which leads to a change in the band gap from 2.56 eV for the initial to 2.52 eV for the irradiated samples. These changes are associated primarily with the formation of additional defects and porous inclusions in the near-surface layer, which lead to the appearance of additional absorbing centers. In this case, a change in the electronic structure of the near-surface layer due to the processes of defect formation and the redistribution of electrons as a result of irradiation leads to a change in the band gap. In the case of low-energy ions, the energy losses in the electron shells and nuclei are of the same order of magnitude, and at high radiation doses, the probability of the effect of overlapping defect regions is approximately 100–1000. Under such conditions, the appearance of defect regions, as well as changes in the electronic subsystem of microparticles, is inevitable, which affects both the optical transmission and the shift of the fundamental absorption edge.

To study the applicability of ionic modification of microparticles in order to increase the photocatalytic activity, as well as comparative analysis, two objects of study were selected: WO_3 microparticles in the initial state and irradiated with helium ions with a dose of 10^{15} ions/cm^2.

Table 1 Crystallographic characteristics of WO_3 microparticles

Parameter	WO_3 microparticles	
	Initial sample	Irradiated 1×10^{15} ion/cm^2
Lattice parameter (Å)	a = 7.2845, b = 7.5176, c = 7.6705, β = 90.91°	a = 7.2961, b = 7.5296, c = 7.6858, β = 91.5°
Density (g/cm^3)	7.33	7.29
Crystalline size (nm)	72.9 ± 5.4	57.4 ± 4.7
Specific surface area (m^2/g)	0.011	0.142
Integral porosity (%)	0.13	0.49
Crystallinity (%)	93.3	92.1

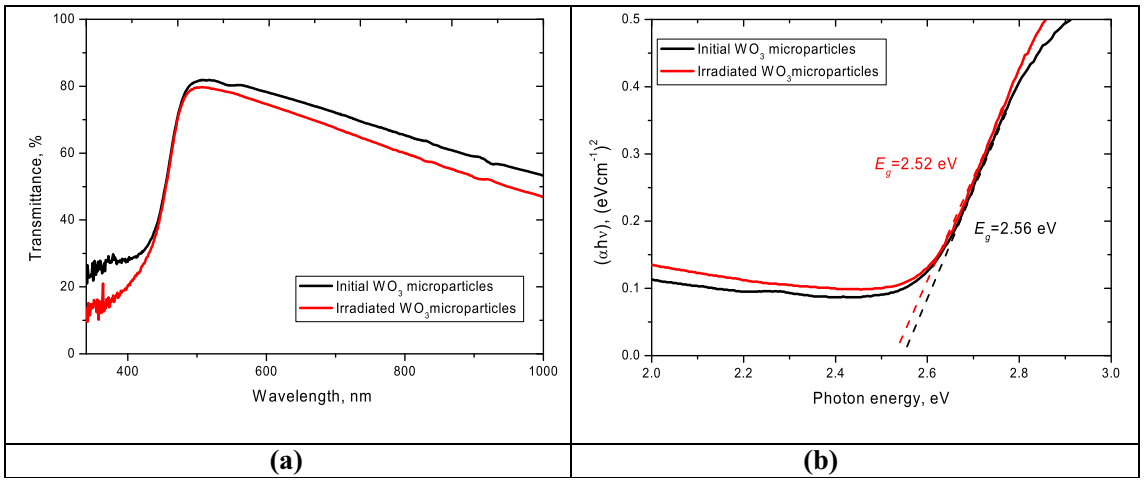

Fig. 5 **a** UV–Vis transmission spectra of the studied WO_3 microparticles; **b** Tauc's plot of WO_3 microparticles

Figure 6 shows the structural formula of Rhodamine B, as well as a schematic representation of the photocatalytic reaction. The choice of the photocatalytic decomposition reaction of Rhodamine B is due to its widespread use in various industries, as well as its solubility in aqueous media, ethanol and methanol. At the same time, the toxicity of Rhodamine B and its solubility makes it one of the most dangerous environmental pollutants. According to the structural formula, Rhodamine B has a complex molecular structure based on aromatic rings and functional groups –COOH, $(C_2H_5)_2N$, $N^+(C_2H_5)_2Cl^-$. According to the photocatalytic reaction scheme, the interaction of Rhodamine B with the photocatalyst occurs due to the presence of a positive charge on Rhodamine B and the negatively charged surface of the microparticles. Moreover, according to the literature [41–45], the larger the specific surface area and the more complex the morphology, the better the interaction between Rhodamine B and the surface.

When irradiated with UV radiation, •OH radicals are formed as a result of absorption of H_2O or –OH microparticles on the surface of microparticles. The main mechanisms with the formation of radicals and subsequent photodegradation are presented below Eqs. (2–4):

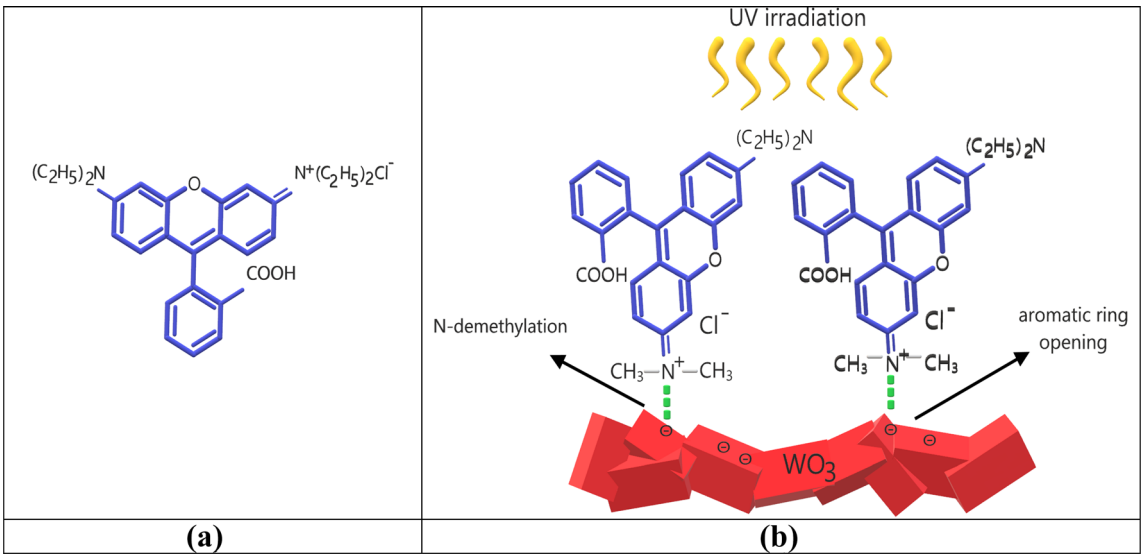

Fig. 6 **a** The structural formula of Rhodamine B; **b** scheme of absorption of Rhodamine B on the surface of WO_3 microparticles through ammonium groups

$$WO_3 + hv \rightarrow e^- + h^+ \quad (2)$$

The formation of radicals:

$$\begin{aligned} H_2O + h^+ &\rightarrow {}^{\bullet}OH + H^+ \\ OH^- + h^+ &\rightarrow {}^{\bullet}OH \end{aligned} \quad (3)$$

Mineralization of organic chemicals:

$$\begin{aligned} \text{Dye} + {}^{\bullet}OH &\rightarrow \text{oxidation products} \\ \text{Dye} + h^+ &\rightarrow \text{oxidation products} \end{aligned} \quad (4)$$

As a result of photocatalytic degradation processes, aromatic rings decompose upon interaction with $^{\bullet}OH$ radicals and subsequent decarboxylation and hydroxylation processes. The final reaction product is harmless components and discoloration of the solutions.

The efficiency of the photocatalytic decomposition reaction of Rhodamine B by WO_3 microparticles in the initial and modified state was determined by measuring the UV spectra in the region of 400–700 nm and evaluating the change in the absorption maximum at 554–556 nm typical of Rhodamine B. The curves of the photocatalytic decomposition reaction were constructed based on concentration analysis changes in the absorption maximum using the formula (5):

$$\text{Degradation\_efficiency} = \left(1 - \frac{C_i}{C_0}\right) \quad (5)$$

where C_0 and C_i are the absorption density before and after the reaction. Figure 7 presents the results of changes in the UV absorption spectra of Rhodamine B depending on the types of catalysts, as well as the dynamics of changes in the photocatalytic degradation curve of Rhodamine B. As an example, the results of changes in the UV spectra of Rhodamine B without adding a catalyst are shown, which showed the absence of any significant changes at the maximum intensity at 554–556 nm. For the initial microparticles, the decrease in the intensity of the maximum absorption occurs in stages and after 300 min of testing does not reach the minimum value, while for the modified microparticles, the discoloration of the solution is observed after 210 min of testing. The mechanism of the photocatalytic reaction is primarily associated with the formation of free electrons and radicals when exposed to UV radiation. In this case, the value of the band gap plays a very important role, since it is it that determines the rate of formation of free electrons due to their release from electron traps. In the case of irradiated samples, for which a decrease in the value of the band gap was observed, as well as a shift of the fundamental absorption edge, which indicates a change in the electron density, the rate of photocatalytic decomposition proceeds much faster.

According to the data obtained, in the case of the initial WO_3 microparticles, the degree of decomposition of Rhodamine B within 300 min reaches no more than 80%, while for modified microparticles, the complete decomposition of Rhodamine B is already observed after 210 min of testing. In this case, the rate constant of the photocatalytic reaction for modified microparticles is 2.3–2.5 times higher than for the initial microparticles. Such a difference in the reaction rate constants and the degree of photodegradation is due to a change in the morphological properties of the surface layer. When irradiated with large doses, the formation of cascade defects is observed, which can lead not only to the displacement of atoms from lattice sites and equilibrium positions, but also to change the electron density, as well as to break crystalline and chemical bonds. As a result, a large number of structural distortions and defects are observed in the near-surface layer, capable of emitting more electrons under the influence of UV radiation, which will accelerate the photocatalytic decomposition and decomposition of Rhodamine B.

Assessment of the dye mineralization and its decomposition into harmless components was carried out by measuring the concentration of Total organic carbon (TOC) in solution depending on the time of the photocatalytic reaction. The dynamics of change is presented in Fig. 8.

As can be seen from the data presented, the degree of mineralization for the initial WO_3 microparticles after 300 min of the photocatalytic reaction was not more than 22%, while the degree of degradation of Rhodamine B during the same time was not more than 80%. In the case of modified microparticles, the degree of mineralization was 47% with complete decomposition and discoloration of the solution as a result of the photocatalytic reaction. According to the obtained data on changes in the TOC concentration, the complete mineralization of Rhodamine B by both the initial and modified WO_3 microparticles is not possible, and the bleaching process may be due to the deethylation of Rhodamine B and the inactivation of chromospheric groups in the dye structure. However, in the case of modified microparticles, the degree of

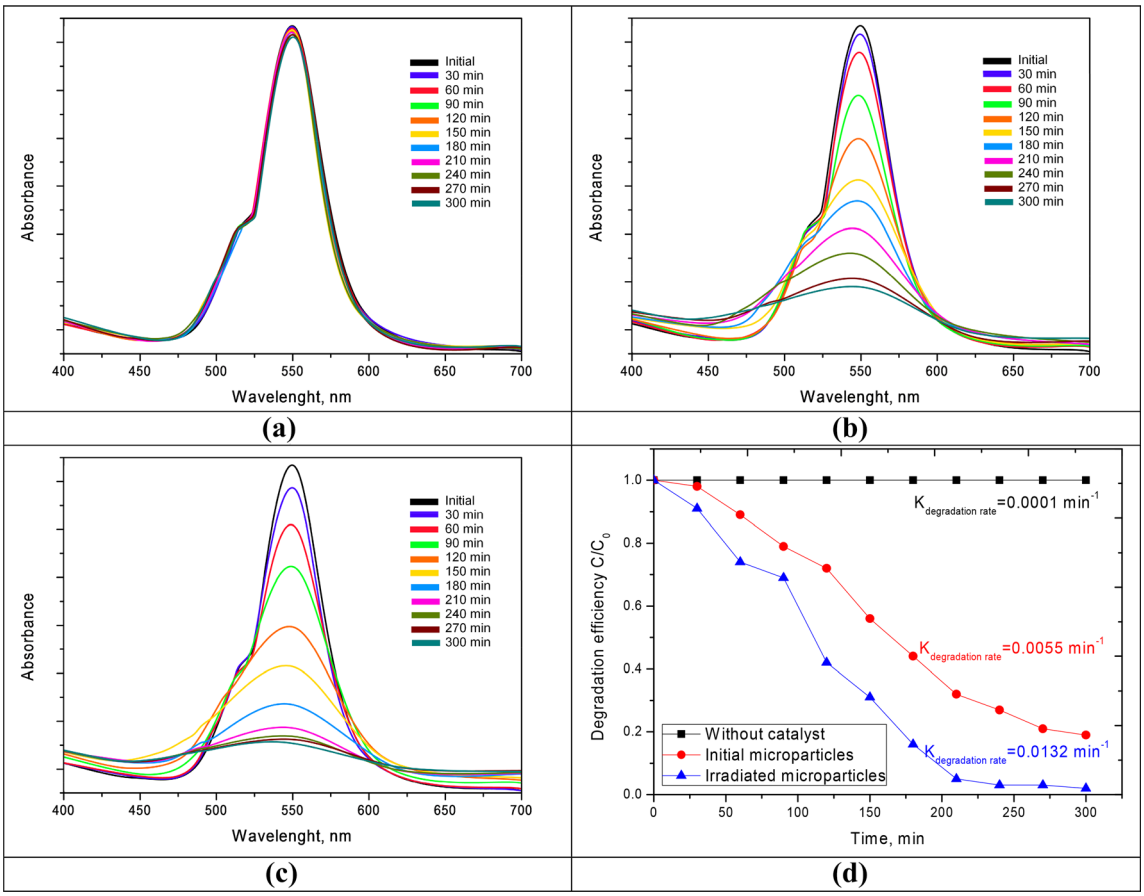

Fig. 7 Dynamics of changes in the UV absorption spectra of Rhodamine B depending on the types of catalysts: **a** without catalyst; **b** WO_3 microparticles in the initial state; **c** WO_3 microparticles after irradiation; **d** dynamics of changes in the photocatalytic degradation curve of rhodamine B (concentration changes were estimated by estimating the absorption maximum at 554–556 nm)

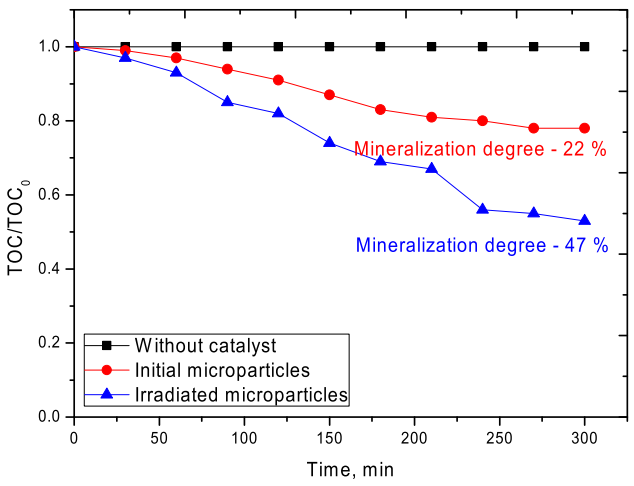

Fig. 8 The dynamics of the concentration of total organic carbon (TOC) in solution as a result of the photocatalytic decomposition reaction

mineralization is more than two times higher than for the original microparticles, which indicates the promise of modification in order to increase not only the photodegradation, but also the mineralization of Rhodamine B.

Figure 9 shows the efficiency diagram for removing chemical oxygen demand (COD) from model media obtained by treating media before and after photocatalytic degradation reactions using the standard dichromate method. In order to increase the efficiency of light transmission through the solution, the concentration of COD was reduced to 630 mg/L. The photodegradation efficiency was estimated according to the formula (6):

$$\eta = \frac{(\mathrm{COD_{initial}} - \mathrm{COD_{final}})}{\mathrm{COD_{initial}}} \times 100\%, \quad (6)$$

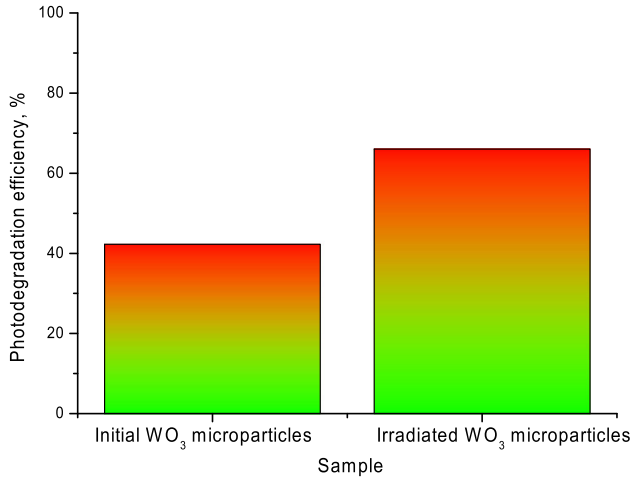

Fig. 9 Diagram of changes in the efficiency of COD removal from aqueous solutions

where $COD_{initial}$ and COD_{final} are COD concentrations in the initial state and after the photocatalytic reaction.

As can be seen from the presented data for the initial microparticles, the COD removal efficiency is about 42–43%, while for irradiated samples this value is more than 65%. The difference in the value of efficiency is associated with a change in the adsorption capacity of microparticles, as well as the specific surface area.

Assessment of the conservation of the efficiency of the degree of photocatalytic decomposition and mineralization of WO_3 by microparticles in the initial and modified state was carried out by successive ten test cycles. Figure 10 presents diagrams of changes in these characteristics over ten cycles.

As can be seen from the data presented, an increase in the number of cycles for the initial WO_3 microparticles leads to a decrease in the degree of degradation and mineralization after seven cycles of consecutive tests. At the same time, for WO_3-modified microparticles, the decomposition efficiency of Rhodamine B is maintained for ten cycles with a slight decrease (no more than 3–5%) after eight test cycles. However, in contrast to the decomposition efficiency, the degradation of the degree of mineralization during the test cycles is more intense and after ten cycles is reduced by 25–30%.

This behavior of the photocatalytic properties indicates a high degree of resistance to lengthy tests, and a decrease in the properties for the initial microparticles may be due to a decrease in strength properties and partial degradation of the surface layer with subsequent crack initiation (see Fig. 11). For modified microparticles, degradation of the surface layer after ten test cycles is practically not observed, which indicates the stability and preservation of the strength characteristics of the modified microparticles. As can be seen from the presented data on the change in the degree of crystallinity of the studied microparticles depending on the number of test cycles (see Fig. 11c), it can be seen that the decrease in the productivity and efficiency of decomposition is due to the formation of amorphous inclusions, as well as partial degradation of the

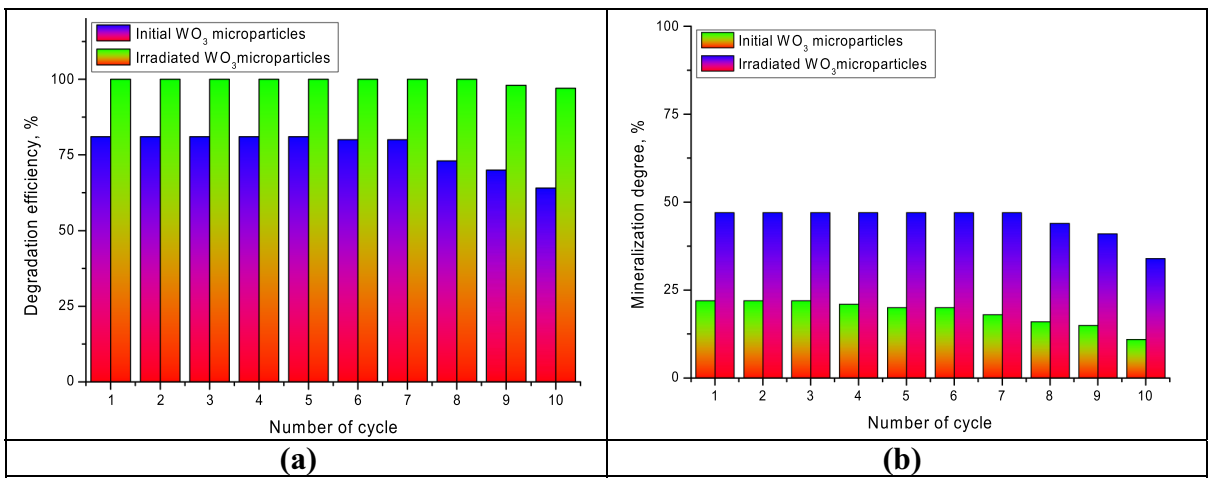

Fig. 10 **a** Dynamics of changes in the degree of degradation depending on the number of test cycles; **b** dynamics of changes in the degree of mineralization depending on the number of test cycles

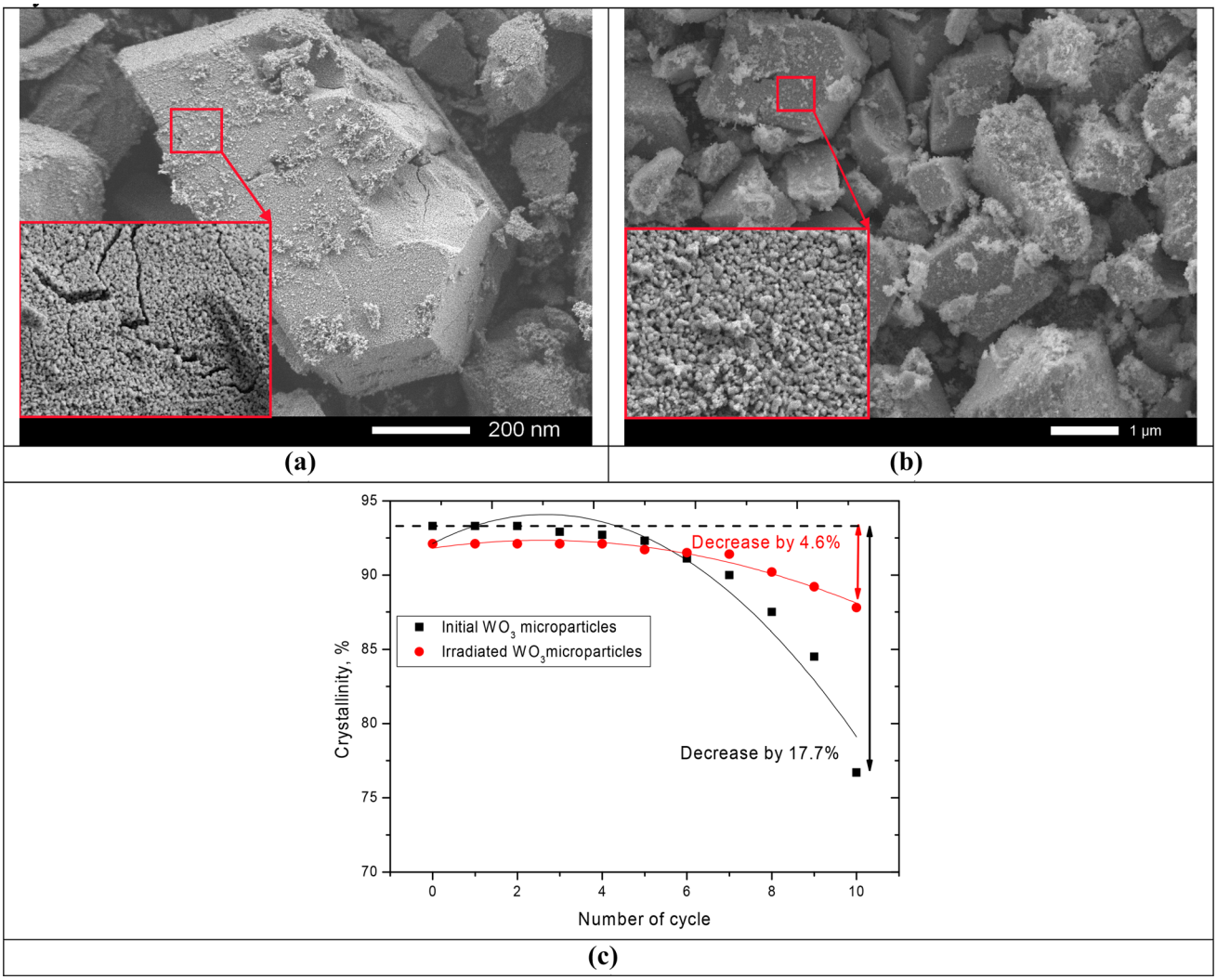

Fig. 11 SEM images of WO_3 microparticles after ten cycles of photocatalytic reactions: **a** initial sample; **b** irradiated 1×10^{15} ion/cm^2; **c** graph of changes in the degree of crystallinity of microparticles depending on the number of cycles

structure. For the initial microparticles, the decrease in crystallinity after ten test cycles was 17.7%, while for the modified microparticles this decrease does not exceed 5%. Thus, it can be concluded that ionic modification leads not only to an increase in the productivity of photocatalytic decomposition, but also to an increase in resistance to degradation during the long-term operation of microparticles.

Figure 12 shows comparative data on the degradation efficiency of Rhodamine B in the case of different modified catalysts based on WO_3. The results of works [45, 55] which consider the effect of doping, as well as various composite structures on the effectiveness of photocatalysis, were selected as comparative data.

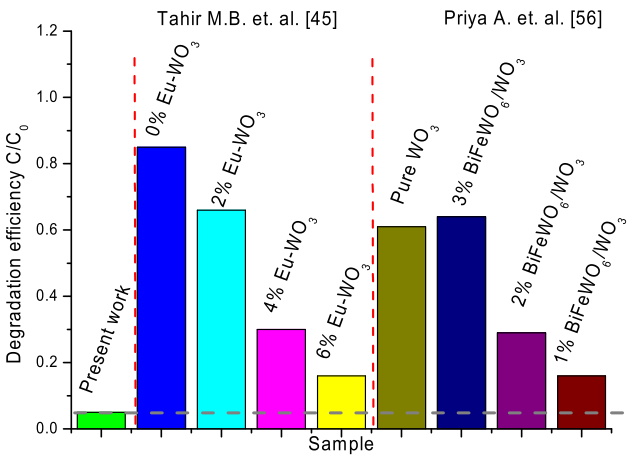

Fig. 12 Comparative diagram of the degradation efficiency of Rhodamine B in the case of different types of catalysts

As can be seen from the presented diagram, the ionic modification of WO_3 microparticles leads to a significant increase in the degree of degradation of Rhodamine B, and is comparable in magnitude, and in most cases even exceeds the doping efficiency. In this case, ionic modification can significantly increase the resistance and durability of microparticles to degradation during long-term use, which also indicates the prospects of using this modification method.

In general, it can be concluded that the obtained results of photocatalytic activity have good agreement with the literary data of photocatalytic properties of nano and microcomposites based on WO_3, as well as its various modifications [55, 56]. At the same time, ionizing radiation is one of the promising methods for modifying the near-surface layer, as well as the electronic subsystem of micro- and nano-particles, along with such methods as doping with rare-earth elements or spinel structures [44, 45, 47, 48, 57–61], changing the specific surface area as a result of reducing particle sizes to nanoscale [62–64], etc. At the same time, unlike doping with rare earth elements or carbon nanostructures, ionic modification allows modifying nano- and microparticles, both commercial type and obtained in laboratory conditions. Modification can be carried out both to change the specific surface area by recrystallization and crushing processes of grains in the near-surface layer, and in order to change the optical and electronic properties of nano- and microparticles. In this case, the modification of the optical and electronic properties can be carried out at a given depth by varying the energy of incident ions, as well as the radiation density. In turn, the scaling of the irradiation technology allows the modification of composite structures on a semi-industrial scale. Also, the proposed technique for modifying catalysts with ionizing radiation can be applied to other types of catalysts based on both thin films and nano- and microparticles.

4 Conclusions

The paper presents the results of the use of low-energy irradiation with helium ions to increase the photocatalytic activity of WO_3 microparticles. Using the methods of scanning and transmission electron microscopy, X-ray diffraction analysis, the dynamics of changes in the morphology and crystallographic parameters of microparticles exposed to irradiation has been established. It was found that irradiation with low-energy helium ions leads to a decrease in the size of crystallites, as well as an increase in the porosity of microparticles by more than 3.5 times. It was found that structural and morphological changes as a result of irradiation lead to an increase in specific surface area by more than ten times.

During experiments with photocatalytic decomposition reactions of Rhodamine B, it was found that the use of irradiation with helium ions leads to an increase not only in the rate of photocatalytic reactions by 2.5 times, but also in the degree of mineralization from 22 to 47%, as well as the efficiency of removing COD from aqueous solutions. Cyclic tests showed the resistance of modified microparticles to degradation, as well as the preservation of decomposition efficiency, while reducing the degree of mineralization after ten test cycles by 30%. At the same time temporary decrease of degree of mineralization for modified microparticles exceeds the degree of mineralization efficiency for initial microparticles, which indicates prospect of application of irradiated microparticles for long cycles of photocatalytic decomposition of organic dyes.

Acknowledgements

The authors thank the Institute of Nuclear Physics of the Ministry of Energy and Science of Kazakhstan for the possibility of conducting experiments on their analytical base.

Author contributions

Conceptualization, MVZ, AA, and ALK; methodology, AA, ALK; formal analysis, MVZ; investigation, AA, ALK and MVZ; resources, MVZ; writing—original draft preparation, review and editing, MVZ and ALK; visualization, MVZ; supervision, MVZ.

Funding

This study was funded by the Ministry of Education and Science of the Republic of Kazakhstan (Grant No. BR05235921).

Compliance with ethical standards

Conflicts of interest The authors declare that they have no known competing financial interests or personal relationships that could have appeared to influence the work reported in this paper.

References

1. H. Zheng, Z.H. Qian, L. Xu, F.F. Yuan, L.D. Lan, J.G. Xu, Switching the recognition preference of rhodamine B spirolactam by replacing one atom: design of rhodamine B thiohydrazide for recognition of Hg(II) in aqueous solution. Org. Lett. **8**(5), 859–861 (2006)
2. T.A. Saleh, V.K. Gupta, Functionalization of tungsten oxide into MWCNT and its application for sunlight-induced degradation of rhodamine B. J. Colloid Interface Sci. **362**(2), 337–344 (2011)
3. M. Sivakumar, A.B. Pandit, Ultrasound enhanced degradation of rhodamine B: optimization with power density. Ultrason. Sonochem. **8**(3), 233–240 (2001)
4. S.C. Yan, Z.S. Li, Z.G. Zou, Photodegradation of rhodamine B and methyl orange over boron-doped g-C_3N_4 under visible light irradiation. Langmuir **26**(6), 3894–3901 (2010)
5. L. Peng, P. Qin, M. Lei, Q. Zeng, H. Song, J. Yang, J. Gu, Modifying Fe_3O_4 nanoparticles with humic acid for removal of rhodamine B in water. J. Hazard. Mater. **209**, 193–198 (2012)
6. T. Wu, G. Liu, J. Zhao, H. Hidaka, N. Serpone, Photoassisted degradation of dye pollutants. V. Self-photosensitized oxidative transformation of rhodamine B under visible light irradiation in aqueous TiO_2 dispersions. J. Phys. Chem. B **102**, 5845–5851 (1998)
7. W. Yao, B. Zhang, C. Huang, C. Ma, X. Song, Q. Xu, Synthesis and characterization of high efficiency and stable Ag_3PO_4/TiO_2 visible light photocatalyst for the degradation of methylene blue and rhodamine B solutions. J. Mater. Chem. **22**(9), 4050–4055 (2012)
8. B. Cuiping, X. Xianfeng, G. Wenqi, F. Dexin, X. Mo, G. Zhongxue, X. Nian, Removal of rhodamine B by ozone-based advanced oxidation process. Desalination **278**(1–3), 84–90 (2011)
9. V.K. Gupta, D. Mohan, S. Sharma, M. Sharma, Removal of basic dyes (rhodamine B and methylene blue) from aqueous solutions using bagasse fly ash. Sep. Sci. Technol. **35**(13), 2097–2113 (2000)
10. N. Barka, S. Qourzal, A. Assabbane, A. Nounah, Y. Ait-Ichou, Factors influencing the photocatalytic degradation of rhodamine B by TiO_2-coated non-woven paper. J. Photochem. Photobiol. A **195**(2–3), 346–351 (2008)
11. H.E. Zhong, Y.A.N.G. Shaogui, J.U. Yongming, S.U.N. Cheng, Microwave photocatalytic degradation of rhodamine B using TiO_2 supported on activated carbon: mechanism implication. J. Environ. Sci. **21**(2), 268–272 (2009)
12. R.A. Al-Samarai, Y. Al-Douri, H. Haftirman, K.R. Ahmad, Tribological properties of WS2 nanoparticles lubricants on aluminum-silicon alloy and carbon steels. Walailak J. Sci. Technol. **10**(3), 277–287 (2013)
13. A.M. Mohammed, R.A. Rahim, I.J. Ibraheem, F.K. Loong, H. Hisham, U. Hashim, Y. Al-Douri, Application of gold nanoparticles for electrochemical DNA biosensor. J. Nanomater. **2014**, 1–10 (2014)
14. K. Byrappa, A.K. Subramani, S. Ananda, K.L. Rai, R. Dinesh, M. Yoshimura, Photocatalytic degradation of rhodamine B dye using hydrothermally synthesized ZnO. Bull. Mater. Sci. **29**(5), 433–438 (2006)
15. R. Jain, M. Mathur, S. Sikarwar, A. Mittal, Removal of the hazardous dye rhodamine B through photocatalytic and adsorption treatments. J. Environ. Manage. **85**(4), 956–964 (2007)
16. K. Gherab, Y. Al-Douri, U. Hashim, M. Ameri, A. Bouhemadou, K.M. Batoo, E.H. Raslan, Fabrication and characterizations of Al nanoparticles doped ZnO nanostructures-based integrated electrochemical biosensor. J. Mater. Res. Technol. **9**(1), 857–867 (2020)
17. Y. Al-Douri, K. Gherab, K.M. Batoo, E.H. Raslan, Detecting the DNA of dengue serotype 2 using aluminium nanoparticle doped zinc oxide nanostructure: synthesis, analysis and characterization. J. Mater. Res. Technol. **9**(5515), 5523 (2020)
18. K. Gherab, C.H. Voon, U. Hashim, M. Ameri, A. Bouhemadou, Aluminium nanoparticles size effect on the optical and structural properties of ZnO nanostructures synthesized by spin-coating technique. Results Phys. **7**, 1190–1197 (2017)
19. K.M. Batoo, E.H. Raslan, Y. Yang, S.F. Adil, M. Khan, A. Imran, Y. Al-Douri, Structural, dielectric and low temperature magnetic response of Zn doped cobalt ferrite nanoparticles. AIP Adv. **9**(5), 055202 (2019)
20. S. Sagadevan, S. Vennila, A.R. Marlinda, Y. Al-Douri, M.R. Johan, J.A. Lett, Synthesis and evaluation of the structural, optical, and antibacterial properties of copper oxide nanoparticles. Appl. Phys. A **125**(8), 489 (2019)
21. M. Salavati-Niasari, Z. Fereshteh, F. Davar, Synthesis of oleylamine capped copper nanocrystals via thermal reduction of a new precursor. Polyhedron **28**(1), 126–130 (2009)
22. Y. Al-Douri, R.A. Al-Samarai, S.A. Abdulateef, A.A. Odeh, N. Badi, C.H. Voon, Nanosecond pulsed laser ablation to synthesize GaO colloidal nanoparticles: optical and structural properties. Optik **178**, 337–342 (2019)

23. Y. Al-Douri, S.A. Abdulateef, A.A. Odeh, C.H. Voon, N. Badi, GaNO colloidal nanoparticles synthesis by nanosecond pulsed laser ablation: laser fluence dependent optical absorption and structural properties. Powder Technol. **320**, 457–461 (2017)
24. Y. Al-Douri, A.A. Odeh, Y.A. Wahab, C.H. Voon, Correlation between magnetization and particle size of CdS nanostructures by solvothermal method. J. Supercond. Novel Magn. **32**(2), 283–289 (2019)
25. N.A. Hamizi, M.R. Johan, Z.Z. Chowdhury, Y.A. Wahab, Y. Al-Douri, A.M. Saat, O.A. Pivehzhani, Raman spectroscopy and FTIR spectroscopy studies of Mn-doped CdSe QDs at different particles size. Optik **179**, 628–631 (2019)
26. K.M. Batoo, G. Kumar, Y. Yang, Y. Al-Douri, M. Singh, R.B. Jotania, A. Imran, Structural, morphological and electrical properties of Cd^{2+} doped $MgFe_{2-x}O_4$ ferrite nanoparticles. J. Alloys Compds. **726**, 179–186 (2017)
27. M. Salavati-Niasari, F. Farzaneh, M. Ghandi, Oxidation of cyclohexene with tert-butylhydroperoxide and hydrogen peroxide catalyzed by alumina-supported manganese(II) complexes. J. Mol. Catal. A **186**(1–2), 101–107 (2002)
28. D. Ghanbari, M. Salavati-Niasari, Synthesis of urchin-like CdS–Fe_3O_4 nanocomposite and its application in flame retardancy of magnetic cellulose acetate. J. Ind. Eng. Chem. **24**, 284–292 (2015)
29. M. Amiri, M. Salavati-Niasari, A. Akbari, Magnetic nanocarriers: evolution of spinel ferrites for medical applications. Adv. Coll. Interface. Sci. **265**, 29–44 (2019)
30. Y. Wu, H. Wang, W. Tu, Y. Liu, Y.Z. Tan, X. Yuan, J.W. Chew, Quasi-polymeric construction of stable perovskite-type $LaFeO_3$/g-C_3N_4 heterostructured photocatalyst for improved Z-scheme photocatalytic activity via solid pn heterojunction interfacial effect. J. Hazard. Mater. **347**, 412–422 (2018)
31. A. Abbasi, D. Ghanbari, M. Salavati-Niasari, M. Hamadanian, Photo-degradation of methylene blue: photocatalyst and magnetic investigation of Fe_2O_3–TiO_2 nanoparticles and nanocomposites. J. Mater. Sci.: Mater. Electron. **27**(5), 4800–4809 (2016)
32. S. Mortazavi-Derazkola, M. Salavati-Niasari, O. Amiri, A. Abbasi, Fabrication and characterization of Fe_3O_4@ SiO_2@ TiO_2@ Ho nanostructures as a novel and highly efficient photocatalyst for degradation of organic pollution. J. Energy Chem. **26**(1), 17–23 (2017)
33. S. Zinatloo-Ajabshir, M. Salavati-Niasari, Z. Zinatloo-Ajabshir, $Nd_2Zr_2O_7$–Nd_2O_3 nanocomposites: new facile synthesis, characterization and investigation of photocatalytic behaviour. Mater. Lett. **180**, 27–30 (2016)
34. M.B. Tahir, H. Kiran, T. Iqbal, The detoxification of heavy metals from aqueous environment using nano-photocatalysis approach: a review. Environ. Sci. Pollut. Res. **26**(11), 10515–10528 (2019)
35. F. Tavakoli, M. Salavati-Niasari, F. Mohandes, Green synthesis and characterization of graphene nanosheets. Mater. Res. Bull. **63**, 51–57 (2015)
36. N.R. Khalid, M. Liaqat, M.B. Tahir, G. Nabi, T. Iqbal, N.A. Niaz, The role of graphene and europium on TiO_2 performance for photocatalytic hydrogen evolution. Ceram. Int. **44**(1), 546–549 (2018)
37. M. Masjedi-Arani, M. Salavati-Niasari, A simple sonochemical approach for synthesis and characterization of Zn_2SiO_4 nanostructures. Ultrason. Sonochem. **29**, 226–235 (2016)
38. M. Yousefi, F. Gholamian, D. Ghanbari, M. Salavati-Niasari, Polymeric nanocomposite materials: preparation and characterization of star-shaped PbS nanocrystals and their influence on the thermal stability of acrylonitrile–butadiene–styrene (ABS) copolymer. Polyhedron **30**(6), 1055–1060 (2011)
39. M. Ahmad, E. Ahmed, Z.L. Hong, W. Ahmed, A. Elhissi, N.R. Khalid, Photocatalytic, sonocatalytic and sonophotocatalytic degradation of rhodamine B using ZnO/CNTs composites photocatalysts. Ultrason. Sonochem. **21**(2), 761–773 (2014)
40. M.A. Mahadik, S.S. Shinde, V.S. Mohite, S.S. Kumbhar, A.V. Moholkar, K.Y. Rajpure, C.H. Bhosale, Visible light catalysis of rhodamine B using nanostructured Fe_2O_3, TiO_2 and TiO_2/Fe_2O_3 thin films. J. Photochem. Photobiol. B **133**, 90–98 (2014)
41. A. Martínez-de la Cruz, D. Sánchez Martínez, E. López Cuéllar, Synthesis and characterization of WO_3 nanoparticles prepared by the precipitation method: evaluation of photocatalytic activity under vis-irradiation. Solid State Sci. **12**(1), 88–94 (2010)
42. D. Martinez, A. Martínez-de la Cruz, E. López Cuéllar, Photocatalytic properties of WO_3 nanoparticles obtained by precipitation in presence of urea as complexing agent. Appl. Catal. **398**(1–2), 179–186 (2011)
43. D. Sánchez-Martínez, A. Martínez-De La Cruz, E. López-Cuéllar, Synthesis of WO_3 nanoparticles by citric acid-assisted precipitation and evaluation of their photocatalytic properties. Mater. Res. Bull. **48**(2), 691–697 (2013)
44. M.B. Tahir, G. Nabi, T. Iqbal, M. Sagir, M. Rafique, Role of $MoSe_2$ on nanostructures WO_3-CNT performance for photocatalytic hydrogen evolution. Ceram. Int. **44**(6), 6686–6690 (2018)
45. M.B. Tahir, G. Nabi, N.R. Khalid, M.M. Rafique, Role of europium on WO_3 performance under visible-light for photocatalytic activity. Ceram. Int. **44**(5), 5705–5709 (2018)
46. W.A.N.G. Cong, C.A.O. Lin, Preparation, spectral characteristics and photocatalytic activity of Eu^{3+}-doped WO_3 nanoparticles. J. Rare Earths **29**(8), 727–731 (2011)

47. M.B. Tahir, M. Sagir, Carbon nanodots and rare metals (RM= La, Gd, Er) doped tungsten oxide nanostructures for photocatalytic dyes degradation and hydrogen production. Sep. Purific. Technol. **209**, 94–102 (2019)
48. K. Shahzad, M.B. Tahir, M. Sagir, Engineering the performance of heterogeneous WO_3/fullerene@Ni_3B/$Ni(OH)_2$ photocatalysts for hydrogen generation. Int. J. Hydrogen Energy **44**(39), 21738–21745 (2019)
49. A.A. Ashkarran, M.M. Ahadian, S.A.M. Ardakani, Synthesis and photocatalytic activity of WO_3 nanoparticles prepared by the arc discharge method in deionized water. Nanotechnology **19**(19), 195709 (2008)
50. S. Adhikari, K.S. Chandra, D.H. Kim, G. Madras, D. Sarkar, Understanding the morphological effects of WO_3 photocatalysts for the degradation of organic pollutants. Adv. Powder Technol. **29**(7), 1591–1600 (2018)
51. S. Leclerc, A. Declémy, M.F. Beaufort, C. Tromas, J.F. Barbot, Swelling of SiC under helium implantation. J. Appl. Phys. **98**(11), 113506 (2005)
52. F. Hofmann, D. Nguyen-Manh, M.R. Gilbert, C.E. Beck, J.K. Eliason, A.A. Maznev, S.L. Dudarev, Lattice swelling and modulus change in a helium-implanted tungsten alloy: X-ray micro-diffraction, surface acoustic wave measurements, and multiscale modelling. Acta Mater. **89**, 352–363 (2015)
53. M.V. Zdorovets, A.L. Kozlovskiy, Study of the stability of the structural properties of CeO_2 microparticles to helium irradiation. Surf. Coat. Technol. **383**, 125286 (2020)
54. M.V. Zdorovets et al., Helium swelling in WO_3 microcomposites. Ceram. Int. **46**(8), 10521–10529 (2020)
55. A. Priya, P. Arunachalam, A. Selvi, J. Madhavan, A.M. Al-Mayouf, Synthesis of $BiFeWO_6$/WO_3 nanocomposite and its enhanced photocatalytic activity towards degradation of dye under irradiation of light. Colloids Surf. A **559**, 83–91 (2018)
56. M.B. Tahir, M. Sagir, M. Zubair, M. Rafique, I. Abbas, M. Shakil, A. Ahmed, WO_3 nanostructures-based photocatalyst approach towards degradation of RhB dye. J. Inorg. Organomet. Polym Mater. **28**(3), 1107–1113 (2018)
57. M.B. Tahir, Construction of MoS_2/CND-WO_3 ternary composite for photocatalytic hydrogen evolution. J. Inorg. Organomet. Polym Mater. **28**(5), 2160–2168 (2018)
58. M.B. Tahir, M. Sagir, N. Abas, Enhanced photocatalytic performance of CdO–WO_3 composite for hydrogen production. Int. J. Hydrogen Energy **44**(45), 24690–24697 (2019)
59. M.B. Tahir, K.N. Riaz, A.M. Asiri, Boosting the performance of visible light-driven WO_3/g-C_3N_4 anchored with $BiVO_4$ nanoparticles for photocatalytic hydrogen evolution. Int. J. Energy Res. **43**(11), 5747–5758 (2019)
60. M.B. Tahir, G. Nabi, M. Rafique, N.R. Khalid, Role of fullerene to improve the WO_3 performance for photocatalytic applications and hydrogen evolution. Int. J. Energy Res. **42**(15), 4783–4789 (2018)
61. M.B. Tahir, Microbial photoelectrochemical cell for improved hydrogen evolution using nickel ferrite incorporated WO3 under visible light irradiation. Int. J. Hydrogen Energy **44**(32), 17316–17322 (2019)
62. M.B. Tahir et al., Synthesis of nanostructured based WO_3 materials for photocatalytic applications. J. Inorg. Organometal. Polym. Mater. **28**(3), 777–782 (2018)
63. M.B. Tahir, G. Nabi, N.R. Khalid, Enhanced photocatalytic performance of visible-light active graphene-WO_3 nanostructures for hydrogen production. Mater. Sci. Semicond. Process. **84**, 36–41 (2018)
64. M.B. Tahir et al., Fabrication of heterogeneous photocatalysts for insight role of carbon nanofibre in hierarchical WO_3/$MoSe_2$ composite for enhanced photocatalytic hydrogen generation. Ceram. Int. **45**(5), 5547–5552 (2019)